# On the Origins of Mass

Moshe Szweizer[1*] and Rivka Schlagbaum[2†]

[1*]Emeritus, Auckland, 1061, New Zealand.
[2]Not Affiliated, Auckland, 1061, New Zealand.

*Corresponding author(s). E-mail(s): mszweizer@gmail.com;
†These authors contributed equally to this work.

**Abstract**

Probability, as manifested through entropy, is presented in this study as one of the most fundamental components of physical reality. It is demonstrated that the quantization of probability allows for the introduction of the mass phenomenon. In simple terms, gaps in probability impose resistance to change in movement, which observers experience as inertial mass. The model presented in the paper builds on two probability fields that are allowed to interact. The resultant probability distribution is quantized, producing discrete probability levels. Finally, a formula is developed that correlates the gaps in probability levels with physical mass. The model allows for the estimation of quark masses. The masses of the proton and neutron are arrived at with an error of 0.02%. The masses of sigma baryons are calculated with an error between 0.007% and 0.2%. The W-boson mass is calculated with an error of 1.3%. The model explains why proton is stable while other baryons are not.

**MSC Classification:** 65C20 , 81P05 , 81P16 , 81Q50 , 37D45

## 1 Introduction

Since the conception of the General Relativity Theorem, the idea of establishing a unified model describing the fundamental forces of nature has become an active research topic. At first, the objective was to unify electromagnetism with gravity. Later, the strong and weak interactions became part of the objective.

Einstein was adamant that a single theory must describe all of nature. In his Nobel lecture in 1923, he said "The intellect seeking an integrated theory cannot rest content

with the assumption that there exist two distinct fields totally independent of each other by their nature". [12]

So it's been more than a century since the search for a unifying theorem became a prominent focus of research. After 100 years of effort, countless research papers, numerous Nobel prizes awarded for the achievements towards that goal, and still a huge pool of intellectual endeavour invested by the giants of scientific thought into this topic, the theory has not been formulated.

Let us pause, step back, and try to understand what has happened. In mathematics, there is a concept of "proof ad absurdum," which is also known as indirect proof or proof by contradiction. When one is unable to prove something directly, one may attempt to show that a negation of the premise does not hold.

At the beginning of the $20^{\text{th}}$ century, this method became part of the physics world due to the problem of establishing the existence of the Luminiferous Ether.

Firstly, the (1887) failed experiment by Michelson and Morley[22], which was being perfected over the following 20 years or so but still failing. This was followed by the 1904 paper by Lorentz[23][24] and, subsequently, the 1905 Special Relativity paper by Einstein[13]. In fact, one may say that the very existence of the Special Relativity Theorem is a direct result of the failed Michelson-Morley experiment.

Thus, the failure of an attempt to establish something became a means to establish the opposite. As a result, proof ad absurdum became part of Einstein's logical vocabulary.

In 1923, Einstein used his enormous influence to rally the scientific community on a quest towards establishing a unified theory. Being able to construct a singular theory of everything effectively disproves the hypothesis of a staged creation of the physical world. Thus, the proof ad absurdum has been set in place. Either the physical reality came about through a singular event or via a number of separate, distinct events.

For the proof ad absurdum to be effective, the scientific community's efforts must fail.

In that instance, a natural question emerges. Specifically, what is the next step? The answer depends on what we would like to discover. Here, we seek the most fundamental principles of physical reality, and it appears that the most fundamental concept is entropy. As such, entropy has been the subject of extensive research. And it appears that entropy may be regarded as the most fundamental component of physical reality.

The investigation of entropic forces constitutes one of the most exciting research topics. This is partly because of the evidence of entropy influencing a wide spectrum of reality, but also due to entropy exerting such influence at the most fundamental levels. In physics, it is expected that entropy provides an agent, which is expressed through the four observable forces of nature [1]. Moreover, entropy has been recognised as a major factor in information transmission theory [2] [3].

Entropic time is associated with entropy production [4] [5] [6], and consequently, the evolution of the universe is associated with entropy production [7]. Entropy is assumed to constitute a fundamental force underlying physically observable reality [8].

Following that line of reasoning, we propose that entropy is the medium enabling the emergence of the property known as inertial mass.

## 2 A note on the Chaos Theory

In mathematics, an infinite sequence of numbers may converge to a specific value, called a limit. A precise definition of a limit was provided by Augustin-Louis Cauchy. The definition assumes that a limit, if it exists for a given sequence, is always a singular number. One of the roots of the chaos theory is the observation that a sequence of numbers may tend to more than one limit, alternatively jumping from one to the next as the sequence progresses. To avoid confusion with the concept introduced by Cauchy, the collection of such limiting numbers is called an attractor, as if to say that these numbers attract the sequence for large n. An attractor can be a singular number, a finite collection of numbers, or an infinite collection, in which case the state while "chaotic" may still be represented through a well-defined orbit.

In many cases, an attractor depends on the initial conditions of the sequence. This leads to the notion of a "basin of attraction". A set of initial conditions that result in the sequence being bounded, belong to the attractors' basin of attraction.[9][10] In turn, the basin of attraction may be split into separate regions, each representing a collection of initial points, which result in the sequence tending to a specific point of the attractor.

## 3 Materials and Methods

The method employs two feedback formulae and runs a looping iteration, feeding the results of each step as input to the next. The question is when to stop the iteration, or, in other words, when to decide that the iteration is close enough to the attractor that it may be terminated. Here, we decided to use a simple rule. If three consecutive values of a sequence are the same, then it is safe to assume that the attractor has been reached and the iteration can be stopped. The experimental observation was that the sequences became stable after no more than 100 steps. We would still run the iteration for 200 steps, but allow the iterating function to terminate when three consecutive values were the same.

In the case of a two-parameter sequence, for an initial point ($p_0$, $q_0$), the sequence is initiated with (1), followed by (2), and (1), etc. This makes the "p" sequence never exposed to the initial condition of $q_0$, as in $q_1(p_0, q_0)$, $p_1(p_0, q_1)$, $q_2(p_1, q_1)$, $p_2(p_1, q_2)$, etc.

The sequence is iterated 200 times, and then, depending on the requirements, either the next 200 iterations or the immediately following value is collected. As (1) is used in the first iteration, the two sequences are asymmetric, with the Q-sequence having an advantage of the first move.

The basin of attraction chart is obtained by setting an equally spaced 1,000x1,000 grid of initial conditions covering the square $(0, 0, p_{max}, q_{max}) = (0, 0, 1.2, 1.2)$. Starting from each initial point, a trajectory is calculated and then evaluated at $k = 2.05$.

To collect data, we ran the script using variables declared as 128-bit long doubles. This resulted in precision as the number of decimal digits at 18, a value range of 3.3621E-4932 to 1.1897E+4932, and epsilon, the smallest number granularity at 1.0842E-19.

# 4 Two Parameter Chaotic Entropy – The Methodology

Let us describe an interaction between two fields, both of which are defined by the Boltzmann-Gibbs entropies and interact with each other via normal conditional relationships.

$$q_{n+1} = P\left(q\,|p\right) = \frac{P\left(q \cap p\right)}{P\left(p\right)} = \frac{-kq_n p_n \ln(q_n p_n)}{p_n} = -kq_n \ln(q_n p_n) \tag{1}$$

$$p_{n+1} = P\left(p\,|q\right) = \frac{P\left(q \cap p\right)}{P\left(q\right)} = \frac{-kq_n p_n \ln(q_n p_n)}{q_n} = -kp_n \ln(q_n p_n) \tag{2}$$

where $0 < \mathrm{k} < \mathrm{e}$ (2.71) and $0 < \mathrm{qp}$

(Note: Here, k stands for a parameter that varies between 0 and Euler's number and does not relate to the Boltzmann constant.)

Formulae (1) and (2) constitute a two-dimensional set of feedback sequences. An important point to note is to observe that the formulae, as they stand, do not impose a limiting value of either q or p. The only constraint is the argument under the logarithm, which must be within the open (0,1) interval (otherwise q or p becomes negative and feeds a negative value to the logarithm's argument). In order to recover probabilities from q and p, we scaled them back by dividing each by their sum. These scaled values are used in the subsequent calculations and shown in the figures.

An example of trajectories obtained through (1) and (2) for a sample of randomly selected initial conditions is shown in Figure 1.

The procedure used in the construction of Figure 1 consists of the following steps:

1. Select a random pair of initial conditions ($q_0$, $p_0$) with values from the (0, 1) interval.
2. Choose a small value of k.
3. Run the sequence (1) (2) for 200 steps, and then collect the subsequent values of ($q_n$, $p_n$) as the attractor.
4. Draw the attractor point(s) with some chosen colour.
5. Increase k by a small step and use the same initial condition for the next run. Again, plot the attractor with the same colour. Repeat until k is close to the Euler's number.
6. Choose another set of initial conditions ($q_0$, $p_0$) and repeat steps 2–5, drawing the results in a different colour.
7. Repeat the above with 20 or so different initial conditions. Plot each set of points in a different colour.

The figure clearly consists of three distinct regions. When k is below 2.0, the attractor is represented by a multiple of points aligned along semi-continuous lines. At k between 2.0 and 2.6, the trajectories asymptotically converge to 0 or 1, without attaining either of these values. When k is above 2.6, the sequences become chaotic, and the attractor consists of a collection of seemingly random points.

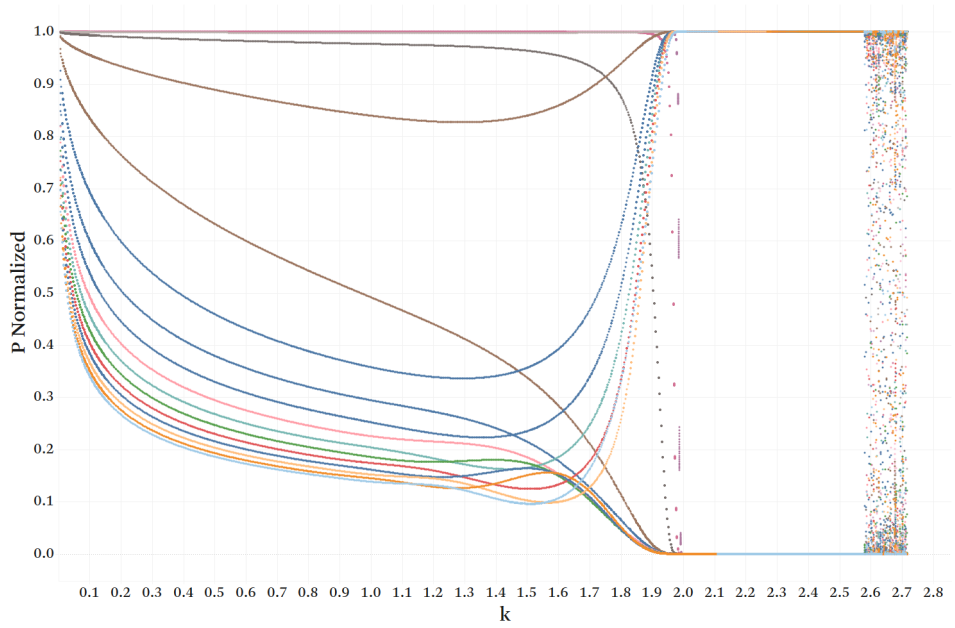


**Fig. 1** An example of p-normalized trajectories

# 5 The banding, error rounding principle and the basin of attraction

The basin of attraction is defined as a collection of initial points that are mapped through the feedback sequence into a specific value of the attractor. It is evident from Figure 1 that for k in the 2.0 to 2.6 range, all trajectories asymptotically tend to the normalized values of either 1 or 0. Therefore, the attractor is either 1 or 0 for k in this interval. Thus, if we demand that the attractor be equal to one of these two values, the collection of the initial points is going to be split into those that lead to 0 and those that lead to 1. Figure 2 illustrates this phenomenon, showing the distinctive banding of the basin of attraction. Here, with k set to 2.1, any initial condition within the green bands leads to the attractors' value of 1, and the initial conditions within the yellow bands lead to the attractors' value of 0.

The error rounding principle is a result of banding and is introduced by observing that, from the attractor's point of view, it is impossible to establish what point within a band was used as the initial condition to arrive at this attractor's value. The breadth of the band limits the most precise estimation that can be established.

To arrive at this estimation, we used the $p_0{=}q_0$ line. This line cuts the bands in their widest region. This allows for the maximal width of each band to be measured, which results in a one-dimensional error-defining parameter.

The next crucial step is the error rounding. One does not consider an error to be a precise number, but rather its magnitude is taken as a representation of its estimation. Therefore, we scale each of the variables by expressing them as multiples of band

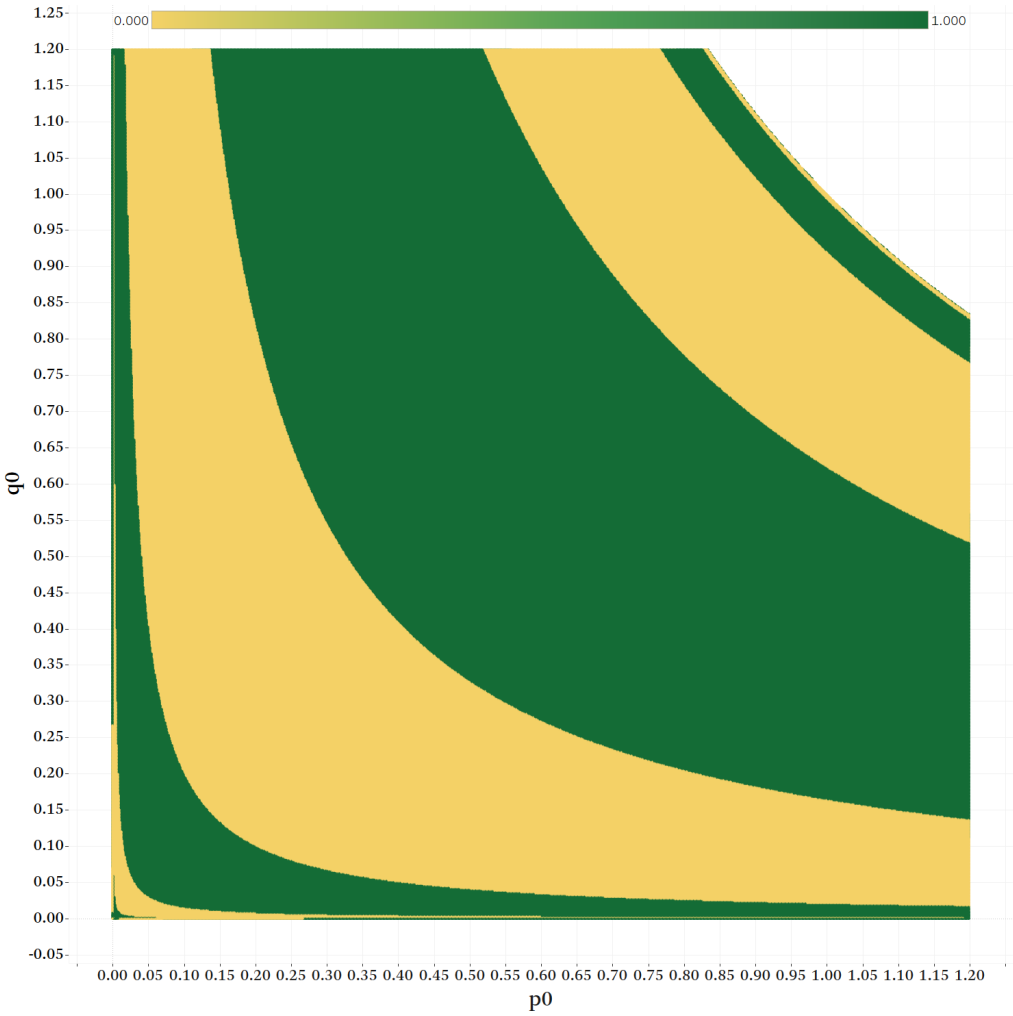


**Fig. 2** Close up of the basin of attraction at k=2.1 and $p_0$, $q_0$ under 1.20 showing attractor bands

width. Another way of looking at this problem is to say that, because of the banding, the most precise knowledge one may have about each of the variables can be expressed as a multiple of the band width.

This approach is applied to the values of p, q, and k variables. Thus, when performing a computation, the sequence is run on a computer at the highest precision available. However, the values used to obtain the normalized p, q, and k are scaled through the banding parameter, as in below. In the case of q and p sequences, the integer portion of the scaling is taken to implement rounding. K is set as multiples of the width of each band, splitting the attractor into a collection of distinctive points along the k-axis. When performing the quantization it is essential that the number is rounded to the nearest integer rather than truncated. This operation mimics the most

naturally expected behaviour; that is, when introducing quantization, the most likely movement would be towards the closest integer. (The formulae for the q-sequence are shown; the p-sequence is similar.)

$$q_{integer} = Integer(rounded)(\frac{q}{(width\,of\,band)}) \tag{3}$$

$$q_{scaled} = q_{integer} * (width\,of\,band) \tag{4}$$

$$k_i = (width\,of\,band) * i \tag{5}$$

Thus, the computed number is divided by the width of the band, rounded to the nearest integer, and then multiplied back by the width of the band to arrive at the scaled value. The scaled value expresses both p and q in terms of multiples of the band width. These values are used to normalise q and p, respectively. The attractor charts are plotted for the normalised values of p-normalised and q-normalised against granulated k, as in (5), (6), and (7).

$$q_{normalised} := \frac{q_{scaled}}{q_{scaled} + p_{scaled}} \tag{6}$$

$$p_{normalised} := \frac{p_{scaled}}{p_{scaled} + q_{scaled}} \tag{7}$$

## 5.1 Basin boundaries and the Lyapunov exponents

Any measurement is subject to error. The most critical measurement here is the width of each band. While those values have little bearing on predicted quark masses, they have a significant impact on computations involving composite particle masses and the W-boson. The inaccuracy stems from the uncertainty surrounding the position of the transition from one band to another. In other words, the width of the edge between each pair of bands is not trivial. The literature refers to this region as a "basin boundary."[16]

Basin boundaries vary depending on the attractor and can be smooth or fractal.[17] In this scenario, the boundaries are smooth, but they broaden the transition between the bands, creating uncertainty in the initial conditions.

Looking carefully at the case considered here, we observe the following: When the initial point is chosen adjacent to the band edge, the sequences 1 and 2 behave asymmetrically. There are locations near the edge where one of the sequences rapidly converges while the other diverges. This behaviour can be studied in depth by examining the Lyapunov exponents for each sequence in the region around the boundary.[18][19]

Lyapunov exponents are a measure of error propagation. They are calculated as the average of consecutive error ratios.[20][21] In particular, if we begin with the starting points $p_0$ and $p_0 + \epsilon$ , where $\epsilon$ denotes a small error, and calculate the images of those two points, the ratio of the post and prior distances between the points and their images, provides a measure of the error change. If the ratio exceeds unity, the error increases; otherwise, it decreases. When calculating Lyapunov exponents, the logarithms of the ratios are averaged. Thus, a positive Lyapunov exponent indicates a diverging sequence, whereas a negative exponent indicates a convergent sequence.

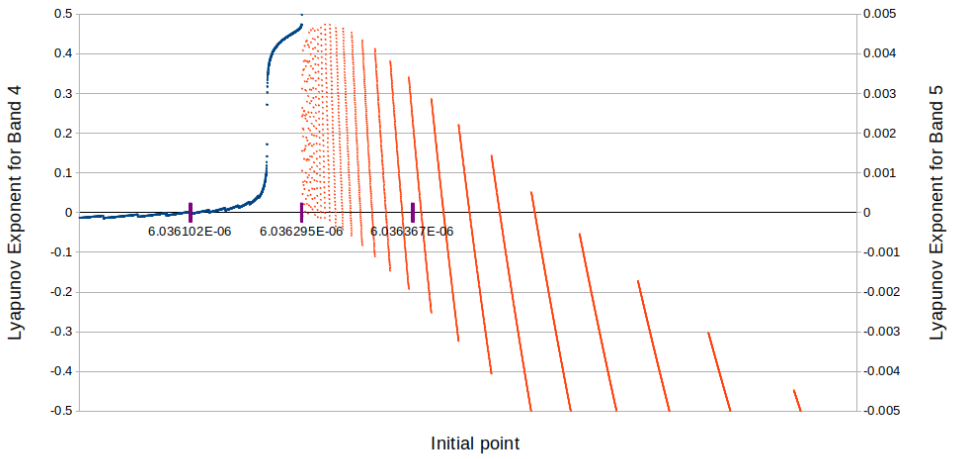


**Fig. 3** Lyapunov exponents at the boundary between bands 4 and 5. Please note different scales.

Figure 3 shows a close-up of the boundary between Bands 4 and 5. Two thousand data points were plotted. Data points were collected when one of the sequences had already converged. The vertical axes depict the Lyapunov exponent for the other sequence. The horizontal axis represents the initial points. Please note that the right axis has a scale that is 100 times finer than the left.

Three points of interest are identified. The boundary point established by the computer is positioned in the middle. The machine indicates this with an accuracy of 19 decimal points. (For all simulations, we used a 128-bit long double data type with an inherent precision "epsilon" of 1.084E-19.) However, Lyapunov exponents change sign some distance from this midpoint, as illustrated in the Figure 3. The numerical results are presented in Table 1.

**Table 1** Zeros of Lyapunov Exponents and Boundary Mid-Points

| Band | Left Zero | Mid-Point | Right Zero | Band | Error |
|---|---|---|---|---|---|
| 2 | 9.525121849042 E-08 | 9.534083887897 E-08 | 9.560245414085 E-08 | 3 | 6.6587 E-19 |
| 3 | 7.853281336832 E-07 | 7.856015230133 E-07 | 7.856800831656 E-07 | 4 | 6.4136 E-19 |
| 4 | 6.036101673169 E-06 | 6.036294834603 E-06 | 6.036367270141 E-06 | 5 | 5.7776 E-19 |
| 5 | 4.288421326183 E-05 | 4.288507096325 E-05 | 4.288489942297 E-05 | 6 | 9.7041 E-19 |
| 6 | 2.787133486889 E-04 | 2.787178081738 E-04 | 2.787178081738 E-04 | 7 | 7.2935 E-19 |
| 7 | 1.634186946017 E-03 | 1.634206556496 E-03 | 1.634206556496 E-03 | 8 | 9.6710 E-19 |
| 8 | 8.483572856683 E-03 | 8.483674660779 E-03 | 8.483674660779 E-03 | 9 | 5.4634 E-19 |
| 9 | 3.797038023000 E-02 | 3.797083588003 E-02 | 3.797083588003 E-02 | 10 | 5.1161 E-19 |
| 10 | 1.407361524549 E-01 | 1.407378413090 E-01 | 1.407372783577 E-01 | 11 | 7.0473 E-19 |
| 11 | 4.038808058157 E-01 | 4.038856524436 E-01 | 4.038856524436 E-01 | 12 | 8.6736 E-19 |
| 12 | 7.881181702138 E-01 | 7.881276277453 E-01 | 7.881276277453 E-01 | 13 | 5.9631 E-19 |
| 13 | 9.586044549117 E-01 | 9.586159583032 E-01 | 9.586159583032 E-01 | 14 | 7.5894 E-19 |
| 14 | 9.952382662828 E-01 | 9.952502092853 E-01 | 9.952462282845 E-01 | 15 | 5.4210 E-19 |
| 15 | 9.996445451943 E-01 | 9.996565410728 E-01 | 9.999804297921 E-01 | 16 | 8.6736 E-19 |

Table 2 lists each band characteristics as measured by setting the trajectories' initial conditions to $p_0$=$q_0$.

**Table 2** Widths of attractor basin bands

| Band Id | Lower Edge $p_0$ | Upper Edge $p_0$ | Attractor | Width of Band |
|---|---|---|---|---|
| 2 | 1.096725463867 E-08 | 9.512901306152 E-08 | 0 | 8.416175842285 E-08 |
| 3 | 9.560245414085 E-08 | 7.853281336832 E-07 | 1 | 6.897256795424 E-07 |
| 4 | 7.856800831656 E-07 | 6.036101673169 E-06 | 0 | 5.250421590003 E-06 |
| 5 | 6.036367270141 E-06 | 4.288421326183 E-05 | 1 | 3.684784599169 E-05 |
| 6 | 4.288489942297 E-05 | 2.787133486889 E-04 | 0 | 2.358284492659 E-04 |
| 7 | 2.787178081738 E-04 | 1.634186946017 E-03 | 1 | 1.355469137844 E-03 |
| 8 | 1.634206556496 E-03 | 8.483572856683 E-03 | 0 | 6.849366300187 E-03 |
| 9 | 8.483674660779 E-03 | 3.797038023000 E-02 | 1 | 2.948670556922 E-02 |
| 10 | 3.797083588003 E-02 | 1.407361524549 E-01 | 0 | 1.027653165749 E-01 |
| 11 | 1.407372783577 E-01 | 4.038808058157 E-01 | 1 | 2.631435274581 E-01 |
| 12 | 4.038856524436 E-01 | 7.881181702138 E-01 | 0 | 3.842325177702 E-01 |
| 13 | 7.881276277453 E-01 | 9.586044549117 E-01 | 1 | 1.704768271664 E-01 |
| 14 | 9.586159583032 E-01 | 9.952382662828 E-01 | 0 | 3.662230797966 E-02 |
| 15 | 9.952462282845 E-01 | 9.996445451943 E-01 | 1 | 4.398316909839 E-03 |

Figure 4 illustrates trajectories for bands 4, 5, and 6 in the region of small k. The error rounding principle results in quantization both along the k-axis as well as p and q normalised values. Now the attractor consists of distinct points, as opposed to the original continuous lines.

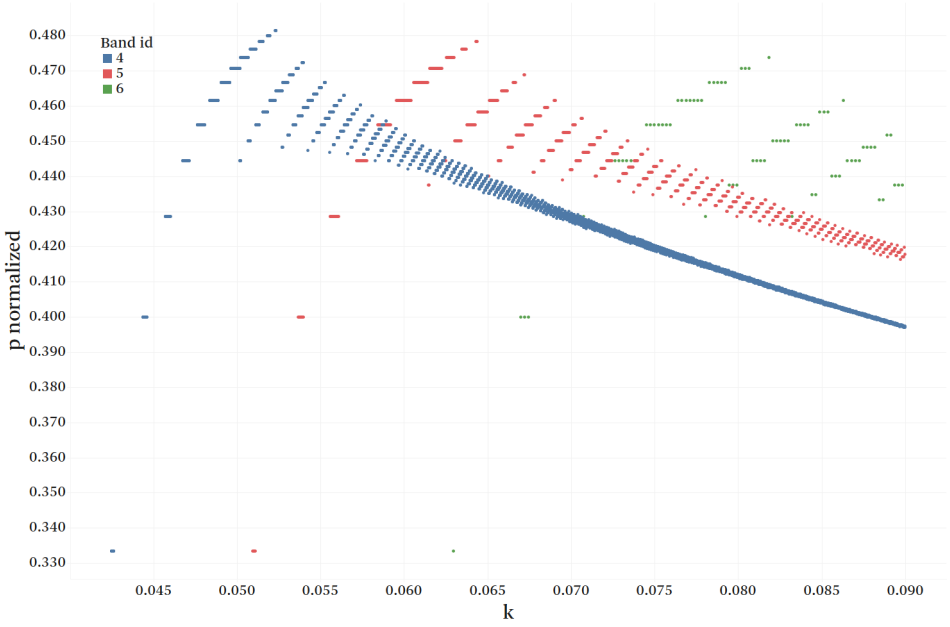


**Fig. 4** Trajectories for bands 4, 5, and 6. The central point of each band was used as the initial condition for each trajectory.

### 5.2 Probability-Mass relationship

Figure 4 shows some form of probability quantization. It would be natural to seek a physical interpretation of this phenomenon as well as a formula that would translate the changes in probabilities into quantities that could be measured physically. In particular, we are interested in how the probability chart could be interpreted in terms of mass.

Let us start with some observations. Firstly, in the very low region of k, when k increases, the probability p also increases. That is, an increase in k results in an entropy increase. So, in light of the Second Law of Thermodynamics, the system should naturally tend to move in the direction of increasing k. We feel strongly that the opposite should be happening. That is, we would like to associate a decrease in k with the system coming to rest. The way to resolve this is to assume that the probability of a particular state should be measured in the context of p-level distances. Thus, the first two levels, with the smallest values of k, have the largest gap between them, so they are the most probable. Moving to the right, the gaps decrease, so the probabilities decrease accordingly.

Secondly, if we were to apply this to mass, then smaller mass should be more probable than heavier mass. Therefore, some form of inverse relationship between probability and mass would be expected. Thus, we would like to assume that mass is related to some form of the inverse of the gap between the adjacent p-levels.

We would like to present a derivation that leads to a functional form we are inclined to use in this context. We are unable to provide a strict derivation of the formula used later on. The best we can present is a general discussion of the expected form of relationship. The actual formula was found by the trial-and-error method.

Firstly (8), we multiply formulae (1) and (2), then (9) substitute "y" for the product of q and p, and finally (10) rearrange to remove the logarithm and replace it with an exponential power. This gives:

$$p_{n+1}q_{n+1} = k^2 p_n q_n (\ln(p_n q_n))^2 \tag{8}$$

$$y_{n+1} = k^2 y_n (\ln(y_n))^2 \tag{9}$$

$$y_n = \exp\left(\frac{1}{k\sqrt{\frac{y_n}{y_{n+1}}}}\right) \tag{10}$$

Based on the formula (10), we would like to seek a relationship between mass and probability through a formula involving an exponent and an inverse of the square root of the line gap.

## 6 The Probability Field and the Quark Masses

The following application of the modelling method allows for the retrieval of the quark masses. The initial conditions are set to $q_0 = p_0$ for each trajectory, with values set in the middle of the band. In Figure 5, the trajectory for the $4^{\text{th}}$ band is plotted, and the locations of the lines relevant to the quark positions are indicated. The k-parameter is run from zero, and the p-normalised values are shown when they depart from null. For values of k where a discontinuity of line is apparent, p-normalised attains a value of

exactly 0.5. This is not shown to enhance clarity. If 0.5 were to be included in Figure 5, the quark levels would resemble energy wells, all starting from a common 0.5 level.

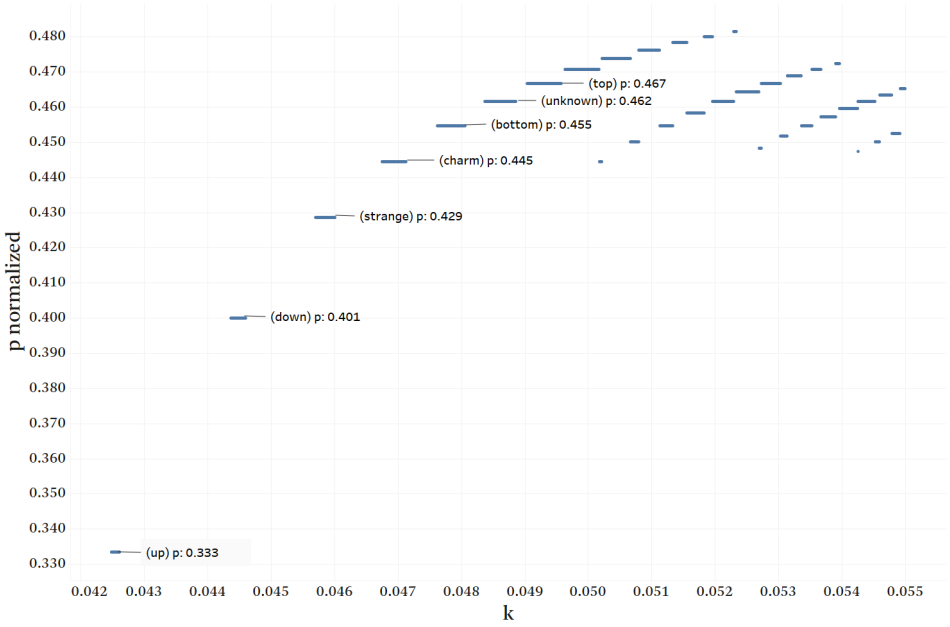


**Fig. 5** The trajectory for band 4 with quark levels

It is assumed that gaining mass is achieved by transiting from each line to the line above. The change in probability is denoted as $\Delta line$. These changes in probability are associated with the mass through (11) and (12), which show that the gain in mass is exponentially proportional to the inverse of the square root of the probability step.

$$M = M_0 \exp(\frac{1}{\sqrt{\Delta line}}) \tag{11}$$

$$where M_0 = 0.15014817 \frac{MeV}{c^2} \tag{12}$$

Formula (11) has not been derived, but rather it is proposed. The authors arrived at this relationship by looking at the chart characteristics and the way the data aligns itself. The scaling constant $M_0$ is found by setting $\Delta line = 2/3$ and assuming that such transition corresponds to the mass of an electron, which is known to eight decimal places.

Table 3 compares quark masses found through the model to those that are experimentally measured. The experimental data is as published by the Particle Data Group [11]. Except for the Down quark and the Top, the values proposed by the model undershoot those found experimentally. The difference is indicated in the deviation column.

The model predicts eight quarks rather than the measured six. Between the Bottom and the Top, an extra quark with a mass of roughly 25 GeV/$c^2$ is expected. Taking into account the data-model relationship's negative bias, its mass has been estimated to be around 28 GeV/$c^2$, as bracketed at ID 6. Another quark (ID 8) with a mass of roughly 1.3 TeV/$c^2$ is also expected.

When k increases further, another set of levels appears beneath the initial one. This terminates the sequence (making the total number of quarks eight) and may point to a later set of distinct particles. IDs 9 to 11 represent the first three in this collection. At this point in the investigation, it is unclear how to interpret any further probability gaps.

**Table 3** The Model and the Experimental results (mass is in MeV/$c^2$)

| ID | K Start | K End | P End | Model | Measured | Dev(%) | Quark |
|---|---|---|---|---|---|---|---|
| 1 | 0.0424856851 | 0.0426116931 | 0.333 | 0.85 | 2.16 | -60.71 | Up |
| 2 | 0.0443705542 | 0.0445963185 | 0.400 | 7.22 | 4.67 | 54.6 | Down |
| 3 | 0.0457041385 | 0.0460086578 | 0.428 | 55.70 | 93.0 | -40.11 | Strange |
| 4 | 0.0467542049 | 0.0471269784 | 0.444 | 420.36 | 1,270 | -66.9 | Charm |
| 5 | 0.04762576 | 0.0480562872 | 0.454 | 3,145.54 | 4,180 | -24.75 | Bottom |
| 6 | 0.0483765574 | 0.0488595879 | 0.461 | 23,438.33 | (28,000) | | Unknown |
| 7 | 0.0490433495 | 0.0495736331 | 0.466 | 174,225.79 | 172,760 | 0.85 | Top |
| 8 | 0.049636637 | 0.0501721709 | 0.470 | 1,293,143.65 | | | Uncharted |
| 9 | 0.0501774212 | 0.0502141735 | 0.444 | 72.86 | | | |
| 10 | 0.0502194239 | 0.0506657021 | 0.473 | 52.04 | | | |
| 11 | 0.0506709524 | 0.0507969604 | 0.450 | 99.66 | | | |

Figure 6 compares experimentally found quark masses with the values proposed by the model. The chart employs a logarithmic scale which produces a straight line for the model.

## 6.1 Other Considerations – the background energy

The model assumes the existence of two distinct probability fields. After normalisation, these are separated by a 0–1 gap, that is, $\Delta$line equals 1, for their respective base lines. Using Formula (11), one can associate this gap with energy (mass) difference of 0.408145 MeV/$c^2$. A natural way of thinking would be to associate this energy with some background energy that is present in all mass-related contexts. It could be called background energy or mass, and it is reasonable to think that it may be related to dark matter.

Furthermore, the charts are symmetric with respect to the normalised p and q. This is due to their definition, which requires them to add up to unity. If one of these variables represented matter, the other would denote antimatter. However, the sequencing always starts with one of the variables (p or q). This disrupts the symmetry of the results. Here, we always begin with the q sequence. If q were associated with matter, antimatter would never form spontaneously.

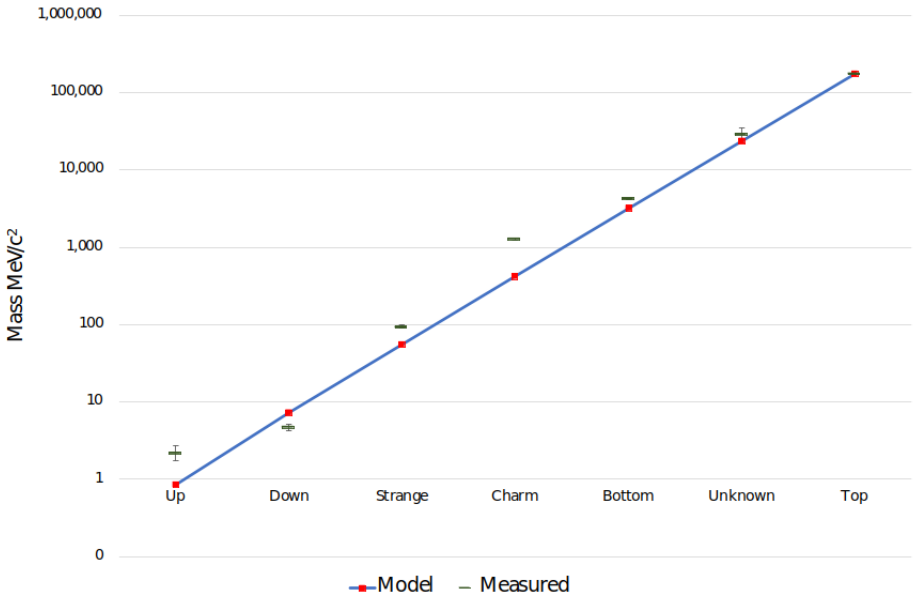


**Fig. 6** Reported and Modelled Quark Masses

# 7 Baryon masses and weak interactions

Bands 4, 5, and 6 allow for the reproduction of the baryon masses. Band 7 does not contain the up quark due to the width of the band. Table 4 summarises the values obtained here and compares them to the experimental data published by the Particle Data Group [11]. A percentage deviation between the model and the experimental results is presented in the last column.

**Table 4** Summary of results

| Particle | Constituents | Model (MeV/c$^2$) | Experimental (MeV/c$^2$) | Difference (%) |
|---|---|---|---|---|
| proton | uud | 938.501 | 938.272 | 0.024% |
| neutron | udd | 939.770 | 939.565 | 0.022% |
| Σ | uus | 1,189.290 | 1,189.370 | -0.007% |
| Σ | uds | 1,193.964 | 1,192.642 | 0.111% |
| Σ | dds | 1,200.335 | 1,197.449 | 0.241% |
| W-boson | W | 79,326.707 | 80,379.000 | -1.309% |

The following is the presentation of the method as applied to each calculation.

## 7.1 Gluons and the probability metric

Quarks interact through the exchange of gluons. This is represented here through a metric (13), which assumes that the interaction requires a gluon's movement along the k-direction and p-direction, both treated as changes in probability, with the absolute

value of the product measuring the amount of the movement. The effective probability is the mean of the movements (14).

$$\Delta_{ij} = |\,(k_j - k_i)\,(p_j - p_i)\,| \tag{13}$$

$$\Delta line = \frac{1}{2}\sqrt{\frac{\sum \Delta_{ij}}{N}} \tag{14}$$

In (14), the summation is over all possible movements, and N stands for the number of combinations.

## 7.2 The composite band error

The calculations are subject to yet another banding-related principle. A baryon consists of three quarks. Each quark is distinct as it is associated with a separate band. The quarks can interact with each other in six ways: (12), (13), (23), (21), (31), and (32). Each interaction involves two moves, one along the k-direction and another along the p-direction, as in (13). Therefore, when calculating the $\Delta line$, there are 12 possible sources of error.

Each movement is subject to an error associated with the width of the band. This error is calculated as the geometric mean of the three widths. Therefore, the maximum error allowed by the movements is 12 times the geometric mean of the widths. This puts a maximum value on the probability of composite particles. Table 5 compares the sum of the quark probabilities (listed in Table 3 in the column labelled "P End") with the maximum error allowed.

**Table 5** Composite band error and the particle constituents' probabilities

| Particle | Quarks | Sum of Quark Levels (P End) | 1 + Max Error | Difference |
|---|---|---|---|---|
| proton | uud | 1.067 | 1.072 | -0.005 |
| neutron | udd | 1.133 | 1.072 | 0.062 |
| Σ | uus | 1.095 | 1.072 | 0.024 |
| Σ | uds | 1.162 | 1.072 | 0.090 |
| Σ | dds | 1.229 | 1.072 | 0.157 |

When one takes a measurement, one allows for a certain degree of error. If the measurement result is within the margin of error, the result is deemed true. In our scenario, we calculate a baryon's composite probability, which is the sum of its three constituent probabilities.

Because the initial conditions were not accurately defined, that measurement has an associated inaccuracy. The breadth of the error is 0.072. In the case of the proton, the constituent probabilities are 2 times 0.333 (up quarks) plus 0.40 (down quark). As a result, the total probability of a proton is 1.066(6), which is greater than one.

That number would appear to be illogical, as probability, by definition, cannot exceed one. However, the measurement error (0.072) surpasses 0.066. As a result, we blame the measurement error for the protons' excess in probability. As a consequence, we may state that the probability of a proton is one while being within the measurement error. Therefore, the proton is stable.

All the other particles listed above have composite probabilities that exceed the measurement error. As a result, they should not appear, and in order for them to exist, even for a brief period of time, something must accommodate the excess in probability. This is also why they must decay.

Table 5 shows that only the proton's total probability imposed through the constituents is less than the maximum error allowed. All other baryons exceed this error, which influences the stability of those particles. This has two consequences. Firstly, the life span of the particle is influenced, with the proton being the only truly stable one. Secondly, in order for the particle to occur, the excess probability must be diverted somewhere.

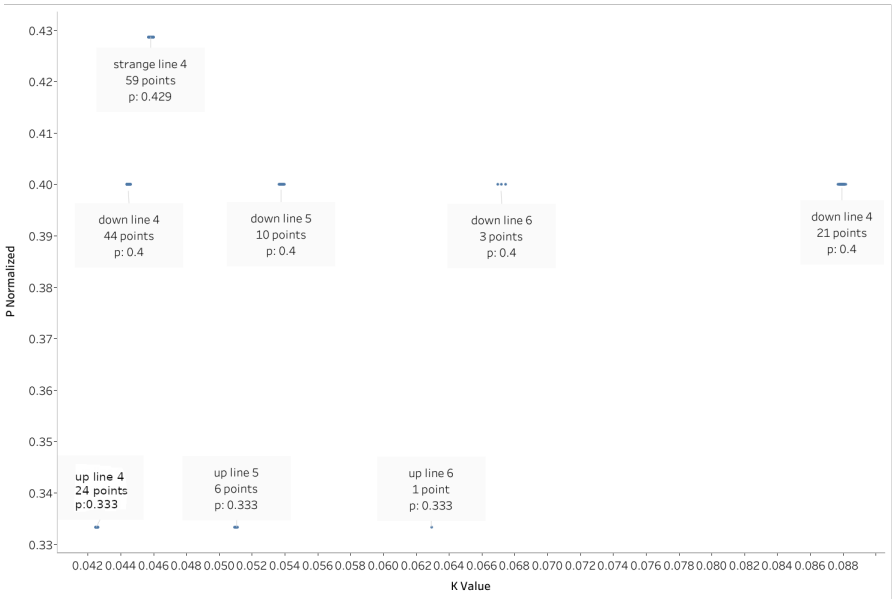


**Fig. 7** Quark lines/trajectories 4, 5, and 6 for up, down and strange quarks as used in calculations

Granulation in the k direction is introduced through (5). The width of k spacing is dependent on the band considered, with the $4^{th}$ band producing the least spaced points and the $6^{th}$ band the most spread out. The number of points is also influenced by granulation. Table 6 lists the number of points on each level, as shown in Figure 7. Only those involved in the subsequent calculations are shown. In the case of the neutron, the down quark on the $4^{th}$ trajectory includes the 21 extended points, as shown in Figure 7 (at k close to 0.09).

## 7.3 Proton – $u_4$ $d_5$ $u_6$

Proton is obtained by placing the first up quark on the $4^{th}$ band, the down quark on the $5^{th}$ band, and the second up quark on the $6^{th}$ band. The number of gluon combinations N is calculated as a sum of pairwise products, giving 10*1 + 10*24 + 24*1 = 274. The

**Table 6** Point counts for levels as in Figure 7

| quark | W | | | neutron | | | proton | | | sigma | | |
|---|---|---|---|---|---|---|---|---|---|---|---|---|
| | 4 | 5 | 6 | 4 | 5 | 6 | 4 | 5 | 6 | 4 | 5 | 6 |
| s - 0.42857 | 0 | 0 | 0 | 0 | 0 | 0 | 0 | 0 | 0 | 59 | 0 | 0 |
| d - 0.40000 | 44 | 10 | 3 | 44+21 | 0 | 3 | 0 | 10 | 0 | 0 | 0 | 0 |
| u - 0.33333 | 24 | 6 | 1 | 0 | 6 | 0 | 24 | 0 | 1 | 0 | 6 | 1 |

line width is calculated with (13). These are entered into (14) and (11), which gives the value of M in (15). To obtain the result listed in Table 4, the proton quark-constituent masses of two down quarks and one up quark are subtracted as in (15).

$$protonmass = M - m_u - 2m_d \tag{15}$$

Please note. The proton is composed of one down and two up quarks, but here the masses of one up and two down quarks are subtracted. Why? Why indeed. Also, in all the calculations, the model-arrived quark masses, as listed in Table 3, are used, not the experimentally found values.

## 7.4 Neutron – $d_4$ $u_5$ $d_6$ including the extension of the 4$^{th}$ band

Neutron is obtained by placing the first down quark on the 4$^{th}$ band, the up quark on the 5$^{th}$ band, and the second down quark on the 6$^{th}$ band. The 4$^{th}$ band is expanded to include points on the closest returning curve, as in Figure 4 and Figure 7 (k in the region of 0.088). The expansion is to partially accommodate the excess of probability. The remaining excess of probability modifies the method of combination counting, which is increased by the maximum amount of the available error. The combinations N are counted as: N = (65*6 + 65*3 + 6*3)* 1.071732166 = 646.254

The redirection of the excess in probability consists of two processes. Firstly, the neutron increases the gluonic activity through the utilisation of the measurement error, but only to its maximum value. In this setting, gluons are more active than the ordinary combination count would have indicated. The remaining excess of probability expands the k range to include the points on the returning branch of the trajectory. The closest points, which are on the 4$^{th}$ band, are therefore included.

To obtain the line width, the summing is calculated over points that include the expanded 4$^{th}$ band. These, together with the expanded combinations count, are entered into (13) and (14).

To obtain the result listed in Table 4, the neutron quark-constituent masses of two up quarks and one down quark are added to (11). As in the case of the proton, the model-calculated quark masses are entered in (16).

$$neutronmass = M + 2m_u + m_d \tag{16}$$

Here, the result is adjusted by involving the masses of two up and one down quarks. As in the case of the proton, this operation is anti-symmetric with respect to the particle constituents. The overall count of the correction and the constituents comes up to the composition of the deuteron, which is stable and, from the quark's composition point of view, balanced.

### 7.5 Sigma – uus, uds, dds

Sigma mass is calculated by placing the strange quark on the fourth trajectory and the two up quarks on the fifth and the sixth. The formula (13) is used in the calculation, with the summing run over each pair of quark locations. This yields the M component, which is corrected by adding the respective quark masses. In each scenario, the strange quark's mass is multiplied by two.

$$\Sigma_{uus} = M + m_u + m_u + 2m_s \tag{17}$$

$$\Sigma_{uds} = M + m_u + m_d + 2m_s \tag{18}$$

$$\Sigma_{dds} = M + m_d + m_d + 2m_s \tag{19}$$

The factor of 2 in the above is understood to account for the strange quark being two levels above the up quark location.

### 7.6 The W Boson u4-d4, u5-d5 and u6-d6 transitions

The mass of the W boson is obtained by limiting the interactions to those that are within each of the three bands. Thus, only $u_4$-$d_4$, $u_5$-$d_5$, and $u_6$-$d_6$ transitions are considered. The line width is calculated using (13) for each transition band independently, and then the results are added together to represent the entire structure. Similarly, the number of combinations is arrived at by adding combinations for each of the bands separately, that is, 44*24 + 10*6 + 3*1 = 1,119. Formula (14) is employed to calculate the effective width and (11) to arrive at the mass listed in Table 4. No other factors are applied in the calculation.

## 8 Discussion

Mass is perceived as something solid (as in tangible and as opposed to abstract). The question being asked is how mass came to be. Therefore, whatever originated mass could not have been solid. In other words, before mass came into being, solidity did not exist. Light is not solid, as it does not have the rest mass. The effect is that photons have to move at the speed of light. However, mass can be stationary. Einstein was motivated by the achievements of his Special Relativity Theorem. Space contraction[13], coupled with the postulation of undistinguishable heavy and inertial mass[14], gave rise to General Relativity. This allowed for the introduction of non-solid curved space-time as an explanation of the solid mass.

It is difficult to escape from a comment we need to make here. Einstein's way of thinking was like that of a pure mathematician. He demonstrated precise reasoning when deriving his theorems, which is a trademark of this approach. It is most evident in the Special Relativity papers[13], but he followed that approach in all of them, including the foundation logic of General Relativity[14][15]. However, when it came to interpretations, he was making errors. Most talked about was the rejection of the probabilistic interpretation of quantum mechanics. Instead, he should have embraced it and applied it to the problems produced by his Special Relativity. If he had done

that, he would have arrived at a more general statement, namely that "physical measurement and objective reality do not have to agree with each other." This discrepancy is evident when one considers a system at its limiting boundary. Like extremely small distances (quantum physics), but also at extremely high speeds (close to the speed of light). In general, one could postulate that this phenomenon occurs always, but in common situations, due to the law of large numbers, it is hidden behind the averages.

In other words, any form of physical measurement has an associated probability. In common experiments, a physicist associates an error estimation with it. Thus, the field of statistics and probability estimation became incorporated into any part of physics, not just quantum mechanics. Here, we have taken another step in that direction, postulating that probability and entropy existed as that 'something' that predates the existence of solidity.

We see mass and light as having different underlying natures. Both of these phenomena must have some origin. However, we would expect that these origins differ in character, resulting in the fundamental difference between mass and light. The prior can be stationary, and the latter lacks that ability.

# 9 Conclusion

The findings presented in the paper are the culmination of years of research into probability and its application to the nature of matter. As our investigation progressed, it became clear that an entirely new philosophical approach was required to confront the failure of the scientific community's quest to establish a unified theory of everything.

The break with the traditional approach to the subject is evident on all fronts. Here we challenge the assumption that inertial and heavy mass are indistinguishable. That assumption was used as the foundation of General Relativity[14]. We break with the notion that entropy is a feature of reality, replacing this with the assumption that entropy is a constituent resulting in physical manifestation. We also discard the traditional mathematical tools used to describe physical phenomena. Instead, we assume that the relationships and mappings that need to be employed are discontinuous, non-differentiable, and chaotic in their nature.

Thus, the work presented here separates inertial mass from other concepts and uses a totally different mathematical framework to describe this phenomenon.

It is postulated here that the inertial mass is a manifestation of two entropic probability fields that interact with each other through conditional probability dependence. This interaction, when quantized, results in probability gaps, which may be associated with the masses of quarks and the electron. In turn, the resultant mass values may be used to reconstruct the masses of elementary particles as measured experimentally.

The model is applied to reconstruct the masses of the proton, neutron, sigma baryon, and W boson. These are provided here as examples to show how the model may be applied. Each calculation differs somewhat from the others, indicating that a certain level of understanding is required in order to apply the model successfully.

# Declarations


- No funds, grants, or other support was received.

- The authors have no competing interests to declare that are relevant to the content of this article.
- All authors certify that they have no affiliations with or involvement in any organization or entity with any financial interest or non-financial interest in the subject matter or materials discussed in this manuscript.

# 10 References


[1] Caticha, A. *Entropic Dynamics* Entropy 2015, 17(9), 6110-6128; https://doi.org/10.3390/e17096110

[2] Shannon, C. E. *Probability of error for optimal codes in a Gaussian channel*, Bell Syst. Tech. J., 1959, vol. 38, pp. 611–656. https://doi.org/10.1002/j.1538-7305.1959.tb03905.x

[3] Verdu, S. *Fifty years of Shannon theory*, IEEE Transactions on Information Theory, 1998, vol. 44, no. 6, pp. 2057–2078. https://doi.org/10.1109/18.720531

[4] Martyushev, L.M.; Shaiapin, E.V. *Entropic Measure of Time, and Gas Expansion in Vacuum.* Entropy, 2016, 18, 233. https://doi.org/10.3390/e18060233

[5] Caticha, Ariel, *Entropic Time*, AIP Conference Proceedings, 2011, 1305, pp. 200–207. https://doi.org/10.1063/1.3573617

[6] Martyushev, L.M. *On Interrelation of Time and Entropy*, Entropy, 2017, 19(7), 345. https://doi.org/10.3390/e19070345

[7] Vilenchik, L. and Vilenchik, M. *The Emergence and Evolution of the Universe*, Journal of High Energy Physics, Gravitation and Cosmology, (2019), 5, 884-898. https://doi.org/10.4236/jhepgc.2019.53044

[8] Wissner-Gross, A. D., and C. E. Freer. *Causal Entropic Forces*, Physical Review Letters, (2013), 110.16. https://doi.org/10.1103/PhysRevLett.110.168702

[9] Feigenbaum, M. *Quantitative universality for a class of non-linear transformations*, J. Statist. Phys. (1978), 19, pp. 25–52. https://doi.org/10.1007/BF01020332

[10] Luque, B., Lacasa, L., Ballesteros, F. J., Robledo, A. *Feigenbaum graphs: a complex network perspective of chaos* PloS one,(2011), 6(9), e22411. https://doi.org/10.1371/journal.pone.0022411

[11] R. L. Workman *et al.* [Particle Data Group], PTEP **2022**, 083C01 (2022) https://doi.org/10.1093/ptep/ptac097 web: https://pdg.lbl.gov/2022/listings/contents_listings.html. Accessed 28 November 2023

[12] Einstein, A. (1923), *Albert Einstein Nobel Lecture. Lecture delivered to the Nordic Assembly of Naturalists at Gothenburg, July 11, 1923*, NobelPrize.org. p. 489 https://www.nobelprize.org/prizes/physics/1921/einstein/lecture/

[13] Einstein, A. (1905), *On the Electrodynamics of Moving Bodies* https://einsteinpapers.press.princeton.edu/vol2-trans/154

[14] Einstein, A., Grossmann M. (1913), *Outline of a Generalized Theory of Relativity and of a Theory of Gravitation* https://einsteinpapers.press.princeton.edu/vol4-trans/163

[15] Princeton University Press, *The Collected Papers of Albert Einstein* https://einsteinpapers.press.princeton.edu/papers Accessed 20 January 2024

[16] Steven W. McDonald, Celso Grebogi, Edward Ott, James A. Yorke (1985) *Fractal basin boundaries* Physica D: Nonlinear Phenomena, Volume 17, Issue 2, 1985, pp. 125-153 https://doi.org/10.1016/0167-2789(85)90001-6

[17] Celso Grebogi and Edward Ott and James A. Yorke (1987) *Chaos, Strange Attractors, and Fractal Basin Boundaries in Nonlinear Dynamics* Science, (1987) 238.4827, pp. 632-638, https://doi.org/10.1126/science.238.4827.632

[18] Sandri, M. (1996). *Numerical calculation of Lyapunov exponents.* Mathematica Journal, 6(3), 78-84. http://www.msandri.it/docs/Numerical_Calculation_of_Lyapunov_Exponents.pdf

[19] Young, L. S. (2013). *Mathematical theory of Lyapunov exponents.* Journal of Physics A: Mathematical and Theoretical, 46(25), 254001. https://doi.org/10.1088/1751-8113/46/25/254001

[20] Geist, K., Parlitz, U., Lauterborn, W. (1990). *Comparison of different methods for computing Lyapunov exponents.* Progress of theoretical physics, 83(5), 875-893. https://doi.org/10.1143/PTP.83.875

[21] Tancredi, G., Sanchez, A., Roig, F. (2001). *A comparison between methods to compute Lyapunov exponents.* The Astronomical Journal, 121(2), 1171. https://doi.org/10.1086/318732

[22] Michelson, Albert A.; Morley, Edward W. (1887). *On the Relative Motion of the Earth and the Luminiferous Ether.* American Journal of Science. 34 (203): pp. 333-345. https://doi.org/10.2475/ajs.s3-34.203.333

[23] Lorentz, Hendrik Antoon (1904), *"Electromagnetic phenomena in a system moving with any velocity smaller than that of light"*, Proceedings of the Royal Netherlands Academy of Arts and Sciences, 6: pp. 809-831

[24] Lorentz, H. A. (1937). *Electromagnetic phenomena in a system moving with any velocity smaller than that of light.* Dordrecht: Springer Netherlands. In Collected Papers: Volume V (pp. 172-197). https://doi.org/10.1007/978-94-015-3445-1_5